Influence of Operating and Physical Variables on Interfacial Area Determination

Fernando Camacho, Emilio Molina, Fernando Valdés, and José Manuel Andujar
Dept. of Chemical Engineering, University of Granada, E-18071 Granada, Spain

The influence of various operating and liquid-phase physical variables on interfacial area a_b in cylindrical and spherical gas-liquid stirred contactors was studied using the sulfite method. Studied were stirring speed, sparger porosity, gas flow rate, liquid-phase temperature, surface tension, and pH.

The results show that the influence of operating variables (gas flow rate Q_g, stirring speed ω, and the average pore radius of the sparger used r_p) on a_b, for both types of contactors, can be given by the equation:

$$a_b = Q_g^{0.5}\left(\frac{k_1}{r_p} + \frac{k_2}{r_p^{1.5}}\,\omega\right)$$

Dependency of a_b on surface tension observed was believed to be caused by a rising rate of bubble coalescence with increased surfactant concentration. The higher the surfactant concentration, the lower a_b, tending to a limit that depends on both the type of surfactant and the average size of sparger pore used. Due to the measurement method used, solution pH and temperature were also observed to influence a_b.

Introduction

From an engineering standpoint, a bubble tank with agitator is very effective in placing gas to be in contact with liquid for both physical absorption and chemical reaction, since liquid residence time and agitation intensity can be varied easily. Furthermore, accurate temperature control is possible because of the relatively high heat transfer coefficient of the contact liquid found in this type of apparatus, especially when process thermal effects are important.

In gas absorption processes, however, even when there is a chemical reaction, process time depends on the mass transfer rate across the liquid interface. Thus, major influence on the gas absorption rate is the dispersion area of the gas-liquid interface. This, in turn, is determined by vessel configuration, impeller speed, gas flow rate, and physical dispersion properties (Robinson and Wilke, 1973).

Most researchers maintain that the specific interfacial area in a stirred bubble tank is a function of the gas speed per unit of free liquid surface, and the power input per unit of volume (Calderbank, 1958), which implicitly includes the influence of the above-mentioned basic variables on a_b

$$a_b = K(P/V)^m(v_s)^n \qquad (1)$$

although discrepancies of $0.3 \leq m \leq 0.45$ and $0.33 \leq n \leq 0.75$ in the values of m and n have been found in the literature.

The influence of the agitation rate on the interfacial area has been studied previously (Westerterp et al., 1963; Yoshida and Miura, 1963; Miller, 1974; Hassan and Robinson, 1977; Matheron and Sandall, 1979; Lineck and Vacek, 1981; Lee and Luck, 1983; Camacho et al., 1988). This influence shows different characteristics in two zones. The first zone is characterized by a low P/V, in which the interfacial area is affected basically by the surface velocity of the gas v_s and the type of agitator used that is practically independent of the agitation rate ω and there is no bubble breakdown. In the second, the bubble breakdown is induced by agitation and higher ω makes bubble size, i.e., the interfacial area, agitation-rate-dependent. The borderline between the two zones is found at an agitation rate ω_c, which depends on the physical properties of the liquid phase and system geometry. Most of the work published deals with high agitation rates (Michael and Miller, 1962; Sridhar and Potter, 1980).

Physical properties of the solution, such as pH, temperature,

Correspondence concerning this article should be addressed to E. Molina Grima, Depto. Ingeniería Química, Campus Universitario de Almería, 04071 Almería, Spain.

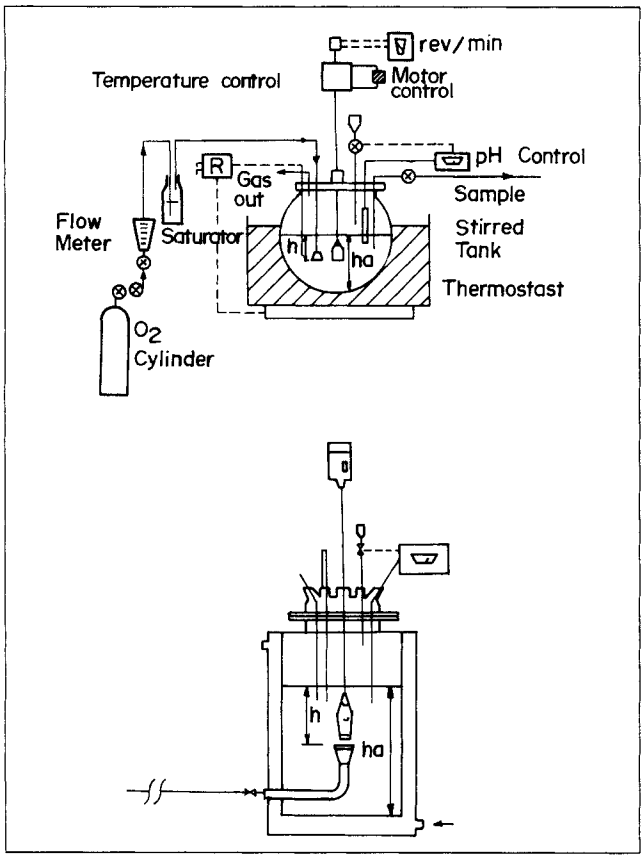

Figure 1. Experimental reactor.

and surface tension, also affect either the actual interfacial area present in the solution or its measurement, and therefore must be taken into account for its correct evaluation. Otherwise, pH may change the active catalyst concentration within the solution and thus the reaction rate, which may lead to erroneous area calculations, even though there is no change in interfacial area. On the other hand, the effect of temperature, which basically influences the reaction rate, on the interfacial area is negligible. Whereas none of these variables affect bubble size or residence time, although they do affect the reaction rate, solution surface tension actually does change equilibrium bubble size and bubble size distribution due to the direct effect of the coalescence rate, as well as side effects such as reducing the mass transfer rate. In this study, interfacial areas were measured using O_2-($SO_3Na_2 + Co^{++}$) and considering the following operating variables: agitator speed, sparger porosity, and oxygen flow rate. Physical properties studied were the liquid-phase temperature, surface tension, and pH. The interfacial areas measured were correlated to these variables for the cylindrical and spherical reactors, as well as two different agitator-sparger arrangements. We arrived at the following conclusions:

- The catalytic specimen is the ion $[Co(OH)^+]$. pH varies its concentration and thus interfacial area measurements. The influence of pH on the interfacial area mentioned in the literature is not related to the variation in $[Co(OH)^+]$ concentration.
- Temperature influences the process according to the theory of Arrhenius and van't Hoff.

Table 1. Parameters of Reactors

Parameters	Spherical	Cylindrical
Reactor Height	0.18 m	0.30 m
Agitator Type*	Centrifugal	Centrifugal
Liquid Level (h_a)	0.10 m	0.19 m
Relative Location Sparger/Stirrer	Same Level Agitator Beside Sparger	Sparger 0.07 m Below Agitator
Free Flat Surface	0.012 m^2	0.019 m^2
Location of Sparger, height (h)	0.05 m	0.05 m
Agitator Radius	0.015 m	0.015 m
Sparger Surface	6.2 $10^{-4} m^2$	6.2 $10^{-4} m^2$

In a previous study (Camacho et al., 1988) the influence of four different types of agitators were investigated and no significant influence of this parameter on the interfacial area was found. The agitator speed used was far below the critical, which for the equipment was 1,900 rev/min (Westerterp et al., 1963). For this investigation, a centrifugal agitator was chosen because it ensured perfect mixing as well as freer liquid surface stability.

- The influence of surfactants depends both on the type of surfactants and the porosity of the sparger, which modify the degree to which bubble coalescence is promoted. Surfactants reduce the interfacial area to a limiting value depending on the initial bubble size produced in the absence of any surfactant and on the kind of reagent used.
- Operating variables affect the interfacial area according to

$$a_b = Q_g^{0.5}\left(\frac{k_1}{r_p} + \frac{k_2}{r_p^{1.5}}\,\omega\right) \tag{2}$$

where k_1 and k_2 are the constants that depend on the physical properties of the solution, tank geometry, and relative placement of the sparger and agitator. Lower than critical agitator speed changes the residence time of bubbles in the solution since it varies the rising speed of bubbles.

Experimental Apparatus and Procedure

Two different reactor arrangements were tested (Figure 1). Table 1 shows the main specifications of the reactors used. The reactors were filled initially with 3 L of sodium sulfite solution to 0.8 M. Variable stirring speeds of the agitator motors of both reactors were set not to noticeably affect the free liquid surface and to remain almost totally flat throughout the experiment.

Oxygen saturated with water vapor and preheated to the required temperature entered the reactor through a perforated plate (sparger) somewhat faster than the maximum rate of absorption measured. Since pH decreases as the reaction progresses, a few drops of concentrated NaOH were added to the solution to keep the pH constant throughout the experiment. pH was controlled with a digital pH-meter. The oxygen absorption rate was determined from the depleted sulfite concentration over a period of time. This concentration never dropped below 0.5 M in any of the experiments. Thus, a flat sulfite concentration profile is guaranteed in the neighborhood of the interface.

Oxygen concentration at the interface $[O_2]_i$ was calculated using Henry's law:

Table 2. Oxygen Diffusivities vs. Temperature

T, °C	DO_2, 10^5 cm^2·s^{-1}
25	1.69
30	1.88
32	1.94
35	2.09
40	2.33

$$[O_2]_i = \alpha P_{O_2} \tag{3}$$

which assumes the usual hypotheses in gas-liquid mass transfer theory (equilibrium solubility is reached and gas-phase resistance is ignored) because of the purity and insolubility of the gas used and the degree of saturation in the liquid phase. The Linek-Vacek relationship (1981) was used to determine solubility α. Partial oxygen pressure, P_{O_2}, was the difference between the atmospheric pressure and the vapor pressure of the sulfite solution at experiment temperature. Liquid-phase oxygen diffusivity, D_{O_2}, was obtained from oxygen diffusivity in pure water, by correcting for electrolytic solutions using the method proposed by Hikita et al. (1979). Calculations for all the temperatures of experimental runs are summarized in Table 2, and experimental conditions are in Table 3. In all experiments, the catalyst concentration varied from 10^{-5} to 4.5×10^{-4} M.

Results and Discussion

In each experiment, the oxygen absorption rate of NO_2A_i was determined by mass balance in the liquid phase and by ignoring accumulation in the bulk liquid, due to low oxygen solubility and fast chemical reaction that takes place. According to this hypothesis, the following equation may be written:

$$NO_2A_i = \frac{V_L}{2}\frac{d[SO_3^=]}{dt} \tag{4}$$

The derivative of the righthand side of Eq. 4 was determined for each experiment by linear regression using the least square method. Variation of sulfite concentration over a period of time was linear, because throughout the experiment the sulfite concentration was greater than 0.5 M. This guarantees a zero-order reaction to the sulfite, whereby the linear fitting can then by applied.

Whenever there is fast reaction oxygen absorption with a flat sulfite concentration near the interface as in these experiments, by the penetration theory, the following equation may be used to determine the oxygen absorption rate:

$$NO_2A_i = [O_2]_i^{\frac{n+1}{2}} A_i \sqrt{\frac{2K_{ap}DO_2}{n+1} + K_\ell^2} \tag{5}$$

where n is the order of reaction to the oxygen.

According to Linek and Vacek (1981), n varies depending on the oxygen concentration at the gas-liquid interface as follows:

- For high oxygen concentration at the gas-liquid interface $[O_2]_i$, the reaction is in the order of 1.
- For low $[O_2]_i$ it is in the order of 2.

When the gas phase is pure oxygen at atmospheric pressure as in these experiments, it is commonly accepted that $[O_2]_i$ is high enough to be considered $n = 1$. With this assumption, Eq. 5 becomes:

$$NO_2A_i = [O_2]_i A_i \sqrt{DO_2k_{ap} + k_\ell^2} \tag{6}$$

where

$$k_{ap} = k'_{ap}[Co^{++}]$$

This equation may be rewritten as:

$$\left(\frac{NO_2A_i}{[O_2]_i}\right)^2 = DO_2k'_{ap}[Co^{++}]A_i^2 + k_\ell^2A_i^2 \tag{7}$$

Thus, by plotting $(NO_2A_i/[O_2]_i)^2$ against $[Co^{++}]$, both effective interfacial area A_i and k_ℓ may be calculated, provided that within the $[Co^{++}]$ range studied, system properties are practically the same (Danckwerts, 1970). Equation 7 is valid only when reaction enhancement factor E_i for the instantaneous reaction

$$E_i = \sqrt{\frac{DO_2}{DSO_3^=}} + \frac{1}{2}\sqrt{\frac{DSO_3^=}{DO_2}}\cdot\frac{[SO_3^=]}{[O_2]_i} \tag{8}$$

is sufficiently higher than the corresponding Hatta number

$$Ha = \frac{(k'_{ap}[Co^{++}]DO_2)^{1/2}}{k_\ell} \tag{9}$$

Assuming that the relationship between diffusivities is not

Table 3. Experiment Conditions

Type Exper.	pH	T, °C	Porosity*	ω rev/min	$Q_g \cdot 10^6$ m^3·s^{-1}	C_l g·L^{-1}
A-1	7.5-10.6	25-40	**	530-932	33.3	0
A-2	8	30	1-4	530	28.3-41.6	3.64×10^{-3} – 4.22
B-1	8	32	1-4	0-1130	28.3	0
B-2	8	32	1-4	530	4.7-70.0	0

A-1 = influence of temperature and pH
A-2 = influence of surfactants
B-1 = influence of agitator speed and porosity
B-2 = influence of gas flow rate
*Average pore radii used were: porosity 1 = 6.45×10^{-6} m; 2 = 3.02×10^{-6} m; 3 = 1.5×10^{-6} m and 4 = 1.00×10^{-6} m.
**Experiment run with known flat interfacial area.

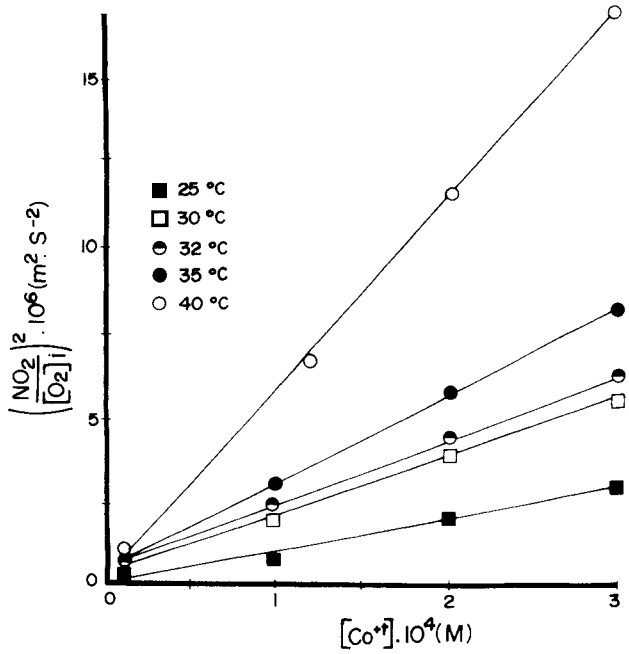

Figure 2. Oxygen absorption rate as a function of catalyst concentration.

Porosity 1, pH = 8, $Q_g = 33.3\ 10^{-6}\ m^3 \cdot s^{-1}$

far from one, the value of E_i for the experiments carried out would vary between 500 and 600, and with average mass transfer coefficient in moderately stirred bubble tanks (2×10^{-4} m^{s-1}) (Charpentier, 1982), the Hatta module varies from 3 to 9. This justifies the low values found on the ordinate at the origin. Thus, Eq. 6 may be used to calculate A_i, provided that the values of k'_{ap} and DO_2 are known.

Equation 7 fits all the results quite well, with negligible amounts at ordinate origin as shown in Figure 2. Interfacial area was calculated from the slopes of similar plots for all the experiments. The specific interfacial area, $a = a_p + a_b$, consists of free liquid area remaining flat throughout the experiment a_p and the area created by the bubbles a_b. For small tanks, a_p is an important fraction of the whole area, which is influenced hardly by operating or physical variables; nevertheless, it was calculated under different operating conditions to assure accurate calculation of a_b.

Influence of Physical Properties

All experiments in this study were carried out using a spherical reactor.

Influence of temperature and pH

In these experiments, there was no gas bubbling in the liquid phase, that is, at known interfacial area a_p, k'_{ap} was calculated by the Danckwert plot method. Figure 3 shows calculated k'_{ap} vs. pH. At any given temperature, the functions relating k'_{ap} to pH show a maximum at pH $\simeq$ 9. This is because of the dissociation balance of Co^{++} in an alkaline medium assuming that this is not the active catalyst, but the ion $Co(OH)^+$. Dissociation balances are:

$$Co^{++} + H_2O \rightleftharpoons Co(OH)^+ + H^+ \qquad (10)$$

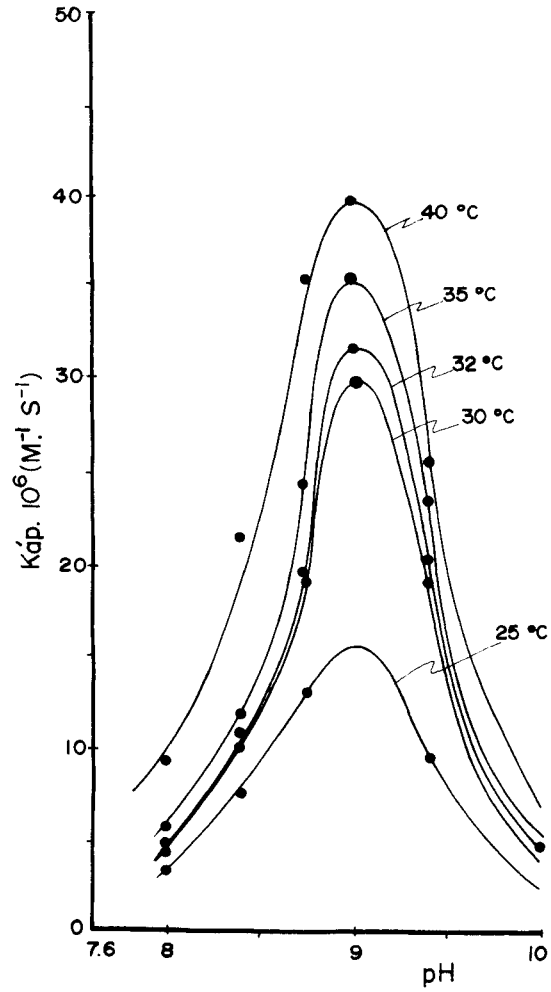

Figure 3. Dependence of k'_{ap} on pH.

The continuous line represents the values obtained with Eq. 15.

$$Co(OH)^+ + H_2O \rightleftharpoons Co(OH)_2 + H^+ \qquad (11)$$

according to Bolzan et al. (1963), who measured the values of these balance dissociation constants in their experiments. Their respective values are:

$$K_1 = 1.41\ 10^{-10}\ M \text{ and } K_2 = 1.26\ 10^{-9}\ M$$

Assuming that c is the total cobalt concentration in any form in the solution, it was used in preparing the solution, and then using Eqs. 10 and 11,

$$c = [Co^{++}] + [Co(OH)^+] + [Co(OH)_2] \qquad (12)$$

From this equation, together with the corresponding analytical expressions for dissociation constants K_1 and K_2, the concentration of ion $|CO(OH)^+|$ can be derived as a function of c

$$[Co(OH)^+] = \frac{c}{1 + \frac{[H^+]}{K_1} + \frac{K_2}{[H^+]}} \qquad (13)$$

in which a maximum is obtained for $[H^+] = \sqrt{K_1 K_2}$. Using

Table 4. Values of k, K_1 and K_2 vs. Temperatures

T, °C	k, 10^{-8} $\times M^{-1}\cdot S^{-1}$	K_2, 10^{10} $\times M$	K_1, 10^{10} $\times M$	Reference
15		1.10	(18.0)*	Bolzan et al. (1963); Sillén (1971)
25		1.41	12.6	Bolzan et al. (1963);
	1.16**	2.77**	17.4**	Sillén (1971)
30		1.94	(10.3)*	Bolzan et al. (1963)
	1.59**	2.88**	23.0**	
32	1.80**	2.97**	25.7**	
35		2.40	(8.3)*	Bolzan et al. (1963)
	2.16**	2.99**	30.2**	
40		3.00	(6.8)*	Bolzan et al. (1963)
	2.90**	3.09**	39.3**	

*Values calculated from literature data.
**Values obtained in this work.

K_1 and K_2 above, $[H^+]_{max} = 9.3$, which agrees with previous data (Roxbourg, 1962; Onda et al., 1970; Yasunishi, 1977). This confirms that the active catalyst is $CO(OH)^+$, whereby

$$k'_{ap}c = k[Co(OH)^+] \tag{14}$$

where k is the actual kinetic constant of the reaction. By manipulating and substituting Eq. 13 to Eq. 14, the following expression relating k'_{ap}, $[H^+]$, K_1 and K_2 is arrived at:

$$\frac{1}{k'_{ap}} = \frac{1}{k} + \frac{[H^+]}{k\cdot K_1} + \frac{K_2}{k\cdot[H^+]} \tag{15}$$

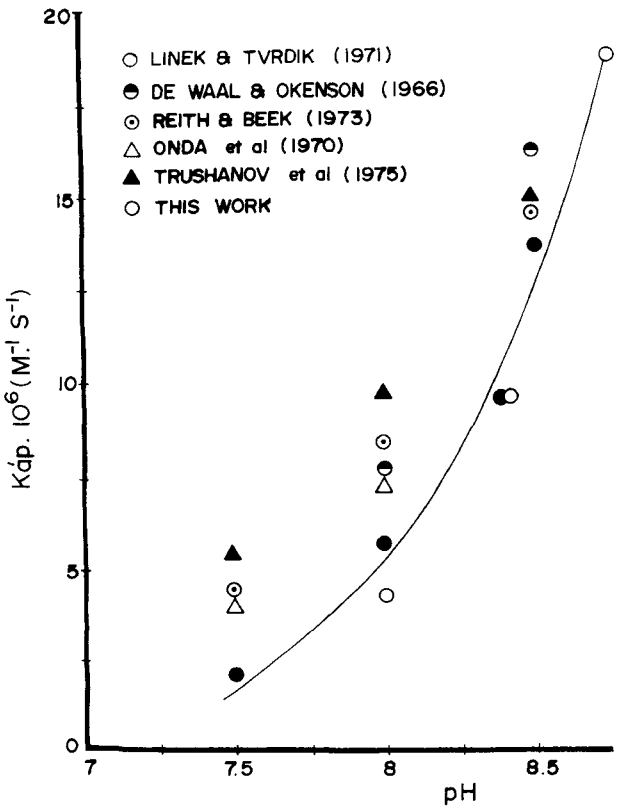

Figure 4. Dependence of k'_{ap} on pH from literature and calculated theoretical predictions.

The experimental values of k'_{ap} in Figure 3 were fit to $[H^+]$ using Eq. 15. A multilinear regression method was used to obtain the values of k, K_1, K_2. Table 4 shows the values thus obtained for the above-mentioned constants. Figure 4 shows the k'_{ap} values found in this study, those calculated from the literature data, and the theoretical prediction calculated with Eq. 15. In spite of the wide deviations among the k'_{ap} values calculated from the literature and the theoretical prediction (possibly due to different reactors and experimental arrangements), it does fit the tendency of the literature data.

The following expressions were found by fitting k, K_1 and K_2 to the temperature with the least square method:

$$k = 2.35\ 10^{16}\ \exp(-5{,}700/T) \tag{16}$$

$$K_1 = 1.03\ 10^{-3}\ \exp(-4{,}603/T) \tag{17}$$

$$K_2 = 42.3\ 10^{-3}\ \exp(-5{,}068/T) \tag{18}$$

showing that the temperature dependence of these constants is the same as that proposed by Arrhenius and van't Hoff. Equations 16 through 18 verify the accuracy of Eq. 15. k'_{ap} has an average relative error of 6.9% with wider deviations at pH close to 9, when the *Ha* number gets so high that Eq. 7 is inapplicable due to the depletion of $[SO_3^=]$ around the interface.

The activating energy E_a from the oxidating and enthalpy reactions for equilibrium in Eq. 10 (ΔH_1) and Eq. 11 (ΔH_2) were calculated from k, K_1 and K_2 in Table 4. These values and those calculated from the literature are shown in Table 5. The ΔH_1 values shown in Table 5 are between 25.92 and 42.64 $kJ\cdot mol^{-1}$ as predicted by Bolzan et al. (1963).

Influence of surfactants

These experiments were carried out with and without oxygen bubbling in the liquid phase. The interfacial areas obtained at different surfactant concentrations are plotted in Figure 5 as a function of concentration.

A clear reduction in a_b with increasing surfactant concentration is evident, especially for the experiments run at porosities of 3 and 4. Not such a strong reduction in a_b is obtained with porosity 1 or those run without oxygen bubbling in the liquid phase; but, in all cases, the specific interfacial area tends to have a limiting value, a_{blim}, when the surfactant concentration surpasses a certain value.

There are two explanations for the behavior observed. A reduction in the product of $DO_2\cdot k'_{ap}$ and/or an increasing rate of bubble coalescence. Because no reduction in the mass transfer coefficient k_ℓ was detected in any of the experiments, var-

Table 5. Values of E_a, ΔH_1 and ΔH_2

E_a kJ/mol	ΔH_1 kJ/mol	ΔH_2 kJ/mol	Reference
49.89	46.11	*	Reith and Beek (1973)
52.41	14.49	*	Trushanov et al. (1975)
51.64	53.45	*	De Waal and Okenson (1966)
47.40	38.10	42.10	This Study

*The experimental data found in literature only allows ΔH_1 to be determined due to the lack of experimental data above pH = 9. Below this pH, the term containing K_2 in Eq. 15 is negligible. Thus, the results of ΔH_2 calculated from it do not merit confidence.

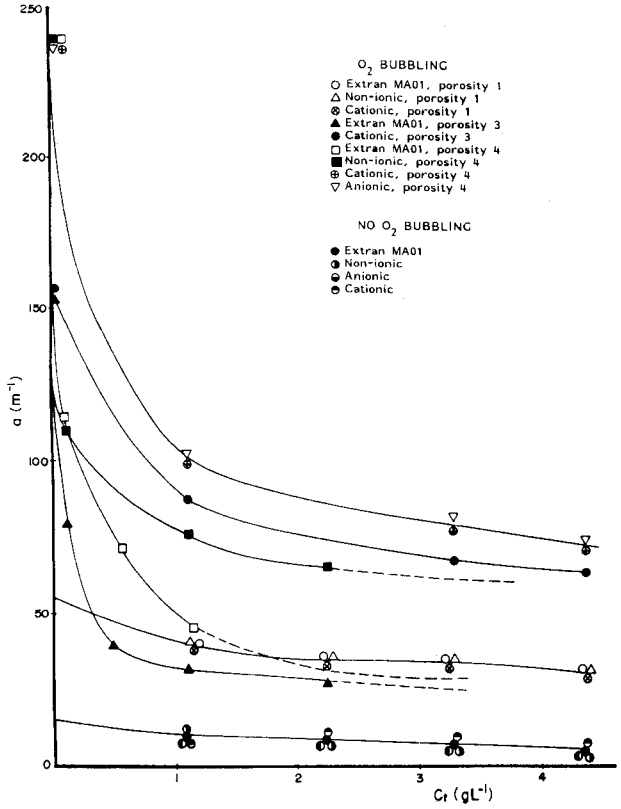

Figure 5. Influence of surfactant concentration on a_b.

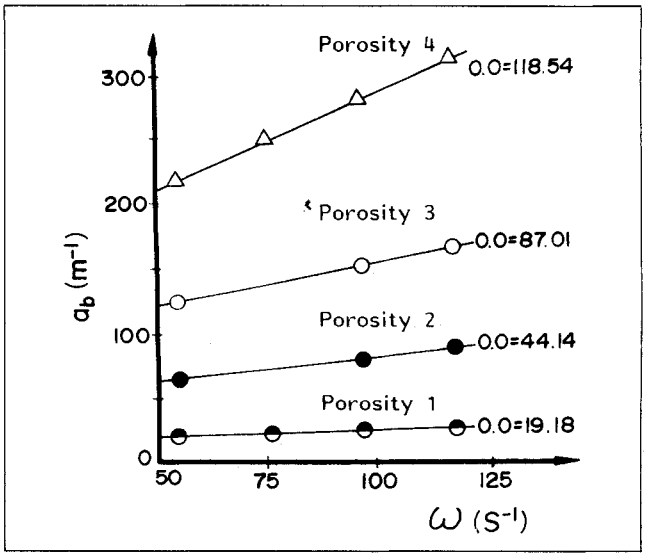

Figure 6. Influence of the stirring speed on a_b.
$Q_g = 28.33\ 10^{-6}\ m^3 \cdot s^{-1}$

iations in interfacial area measurements of those run at porosity 1 and without oxygen bubbling through the liquid phase were thought to be attributable to the same cause, the decrease in the product of $DO_2 \cdot k'_{ap}$.

The behavior observed with porosities 3 and 4, however, cannot be explained in terms of the reduction of the product $DO_2 \cdot k'_{ap}$, for which the strongest effect must be assumed. This can only be due to the increasing bubble coalescence rate as the surfactant concentration increases. As deduced from Figure 5, the coalescence rate stabilizes at a relatively low surfactant concentration, producing a bubble size that depends both on the surfactant and porosity used, showing that the presence of a surfactant increases coalescence. This offers bubbles tendency to a size limit, a_{blim}, corresponding to the formation of a single layer of the surfactant at the interface.

From the shape of the curves in Figure 5, the following relationship between bubble area and surfactant concentration is valid for experiments with porosities 3 and 4.

Table 6. Values of C_1 and C_2 Corresponding to Eq. 22

Surfactant*	C_1	C_2
Nonionic	0.48	−1.69
Extran	1.05	−2.69
Cationic	2.68	−48.16
Anionic	1.15	−44.54

*Nonionic surfactant: lauryl alcohol 4.0E (moles of OE 3.6; hydrophobic chain 75% C_{12}, 1.2% C_{13}, 20% C_{14}, 3% C_{16} and free polyglycols 0.08%); cationic surfactant: N-cetyl-N,N,N-trimethyl-ammonium bromide $C_{19}H_{42}BrN$; anionic surfactant: Sodium dodecyl hydrogen sulfate: $C_{12}H_{25}NaSO_4$; commercial surfactant: Merck, Acaline Extran MA01.

$$a_b = a_{blim} + \beta \exp \alpha(c_t) \tag{19}$$

Since as porosity increases (average pore radius diminishes) the speed at which bubble area approaches its limit is greater (see Figure 5), a_b depends on the initial size of the bubble generated, that is, the area at zero surfactant concentration, so that β may be reasonably expressed as:

$$\beta = a_{bo} - a_{blim} \tag{20}$$

making the relationship between a_b and surfactant concentration,

$$\frac{a_b - a_{blim}}{a_{bo} - a_{blim}} = C_1 \exp \alpha(c_t) \tag{21}$$

where C_1 is a constant yet to be determined.

Potential functions were tried for $\alpha(c_t)$ in the form of $\alpha(c_t) = C_2 C C_t^n$ and a good fit of experimental values for $n = 0.5$ was obtained. Equation 21 therefore becomes:

$$\frac{a_b - a_{blim}}{a_{bo} - a_{blim}} = C_1 \exp C_2 C_t^{0.5} \tag{22}$$

Constants C_1 and C_2 calculated using the least square method are summarized in Table 6 for each surfactant used.

Equation 22 reproduces the a_b values obtained in experiments at porosities 3 and 4, with a relative error lower than 3.5% for nonionic, anionic and cationic surfactants, increasing up to 7% for the commercial surfactant Extran MA01.

Influence of operating variables

To determine the influence of operating variables on the interfacial bubble area, oxygen was bubbled into the media in the liquid phase. Variables studied were the following:

- Gas flow rate
- Agitator speed
- Sparger porosity

Influence of sparger porosity and stirring speed

Interfacial areas for the spherical reactor obtained at constant oxygen flow rates are plotted against the agitator speed by porosity in Figure 6. In this figure the influence of these two variables is seen to be inseparable and should be considered simultaneously, the dependence of a_b on them being expressed as:

$$a = a - a_p = \alpha(r_p) + \beta(r_p)\omega \tag{23}$$

In theory, if there is no bubble breakdown due to agitation, $\alpha(r_p)$ should represent the interfacial area obtained at $\omega = 0$. The interfacial areas obtained in the experiments without agitation performed to confirm this hypothesis were: porosity 1, $a_b = 18.1\ m^{-1}$; porosity 2, $a_b = 43.48\ m^{-1}$; porosity 3, $a_b = 83.38\ m^{-1}$; and porosity 4, $a_b = 124.72\ m^{-1}$. These values agree reasonably well with those of the ordinates at the origin, 0.0, in Figure 6 leading to the following conclusions.

1. Equation 23 can explain the influence of the agitator speed on a_b within the whole range used in this study $0 \le \omega \le 1{,}130$ rev/min.

2. Agitation does not break down the bubbles.

$\alpha(r_p)$ and $\beta(r_p)$ were determined using the least square method with the following results:

$$\alpha(r_p) = (a_b)_{\omega=0} = k_1 \cdot r_p^{-1} \tag{24}$$

$$\beta(r_p) = k_2 \cdot r_p^{-1.5} \tag{25}$$

whereby the relationship between a_b, ω and r_p is found to be:

$$a_b = \frac{k_1}{r_p} + \frac{k_2}{r_p^{1.5}}\omega \tag{26}$$

Influence of oxygen flow rate

In Figure 7, a_b has been plotted against $Q_g^{1/2}$ for each of the porosities used. From this plot, the following expression may be derived:

$$a_b = k\ Q_g^{0.5} \tag{27}$$

where k is a function of both porosity and agitator speed (Camacho et al., 1988),

$$k = \frac{k_1}{r_p} + \frac{k_2}{r_p^{1.5}}\omega \tag{28}$$

and substituting Eq. 28 into Eq. 27, the following expression is obtained for a_b:

$$a_b = Q_g^{0.5}\left(\frac{k_1}{r_p} + \frac{k_2}{r_p^{1.5}}\omega\right) \tag{29}$$

Results of experiments with a cylindrical reactor using the sparger-stirrer arrangement in Figure 1 show that the variation of interfacial area with the above-mentioned variables is similar to those obtained in the spherical reactor, except for the agitator speed which affects it negatively, Figure 8. Equation 29

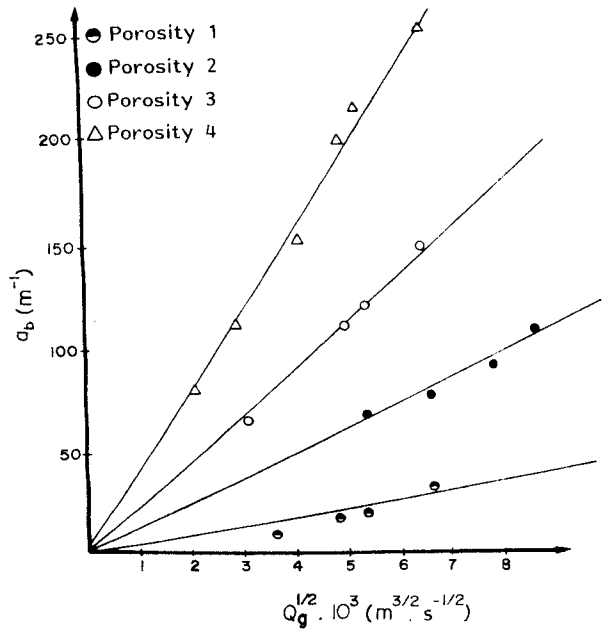

Figure 7. Influence of the oxygen flow rate on a_b.

ω = 530 rev/min

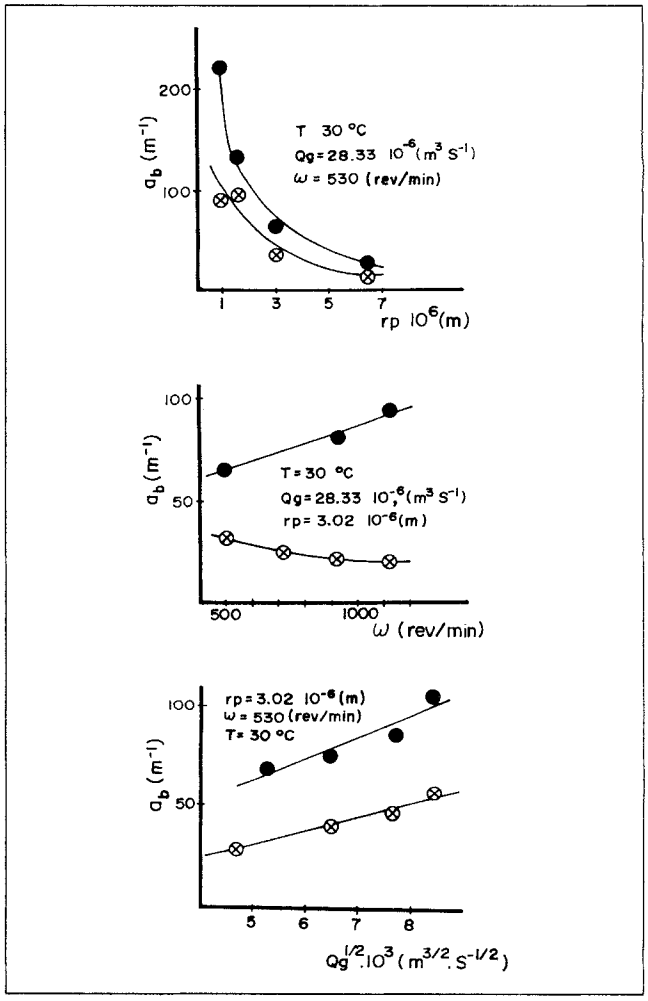

Figure 8. Influence of the operational variables on a_b.

●, spherical reactor; ⊗, cylindrical reactor

Table 7. Values of Constants Relating the Specific Interfacial Area to Operating Variables in Spherical and Cylindrical Stirred Tanks

	Spherical Reactor	Cylindrical Reactor
k_1	0.023	0.016
k_2	$2.79\ 10^{-7}$	$-4\ 1310^{-8}$

fits these experimental values as well, although the values of k_1 and k_2 differ from those obtained with the spherical reactor (See Table 7).

Equation 29 reproduces the values of a_b obtained in this study for both spherical and cylindrical reactors with an error of less than 10%. The interfacial area obtained in this work has also been correlated to the operating variables using a Calderbank-type equation (Eq. 1) with the values for k, m and n of 16.01, 0.4 and 0.5, respectively. Equation 1 reproduces our results with an error of less than 20%, which is double the error obtained with Eq. 29. This equation consists of two terms, T_1 and T_2:

$$T_1 = K_1 \frac{Q_g^{0.5}}{r_p} \text{ and } T_2 = K_2 \frac{Q_g^{0.5}}{r_p^{1.5}} \omega \qquad (30)$$

The first term, T_1, represents the dependence of a_b on the operating variables currently found in the literature, when the agitator speed used in the experiment is below the critical ω_c, at which bubble breakdown starts. The second term, T_2, is due to the variation in bubble retention time induced by the distribution in liquid produced by currents of agitation. This current distribution should be similar to that in Figure 9. In the spherical reactor, bubbles are produced where the currents induced hinder the rising movement of the bubbles produced, thus increasing bubble residence time in the solution and consequently increasing the number of bubbles within the liquid phase, to which a_b is directly proportional. In the cylindrical reactor, the currents induced favor the rising movement of the bubbles, hence disminishing the bubble residence time and, consequently, the interfacial area.

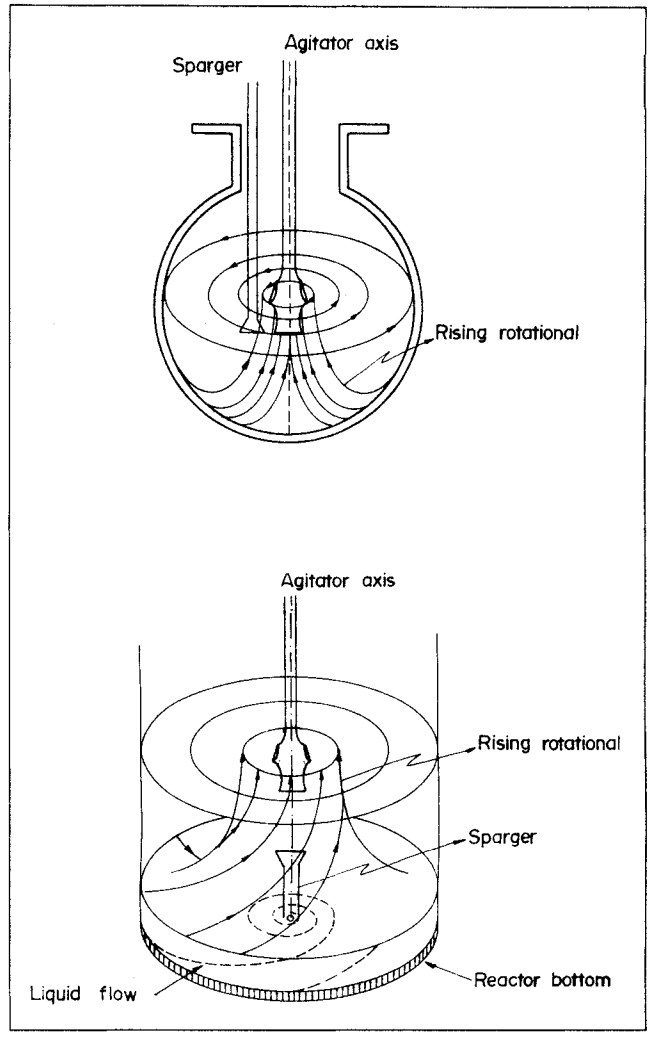

Figure 9. Fluid dynamic situations considered inside each reactor type.

Notation

a = specific interfacial area, m^{-1}
a_b = specific bubble interfacial area, m^{-1}
a_{bo} = bubble interfacial area at zero surfactant concentration, m^{-1}
a_p = specific interfacial area of free liquid surface, m^{-1}
A_i = interfacial area, m^2
c = total cobalt concentration, M
C_t = surfactant concentration $g \cdot L^{-1}$
C_1 = constant in Eqs. 21 and 22
C_2 = constant in Eq. 22
D_{O_2} = oxygen diffusivity, $cm^2 \cdot s^{-1}$
D_{SO_3} = sulfite diffusivity, $cm^2 \cdot s^{-1}$
h = sparger location in height, m
h_a = liquid level, m
Ha = Hatta number
k = kinetic constant of the chemical reaction, $M^1 \cdot s^{-1}$
k_{ap} = apparent pseudo first-order kinetic constant, s^{-1}
k'_{ap} = apparent second-order reaction kinetic constant, $M^1 \cdot s^{-1}$
k_t = mass transfer coefficient, $m \cdot s^{-1}$
k_1 = constant in Eq. 29
k_2 = constant in Eq. 29
K = constant in Eq. 1
K_1 = equilibrium constant, Eq. 10, M
K_2 = equilibrium constant, Eq. 11, M
N_{O_2} = oxygen absorption rate, $mol \cdot s^{-1}$
P_{O_2} = partial oxygen pressure, atm
Q_g = gas flow rate, $m^3 \cdot s^{-1}$
r_p = average pore radius, m
T = temperature, K
V_t = liquid volume, m^3
v_s = superficial gas velocity, $m \cdot s^{-1}$

Greek letters

α = Henry's law constant, $M \cdot atm^{-1}$
$\alpha(\ )$ = proportionality in Eqs. 19, 21, 23 and 24
$\beta(\ )$ = proportionality in Eqs. 23 and 25
ω = stirring speed, rev/min or s^{-1}

Literature Cited

Bolzan, J. A., J. J. Podesta, and A. J. Ariva, "Equilibrio Hidrolítico de Iones Metáalicos: I. La Hidrólisis del Ión Co(II) en Soluciones Acuosas de $NaClO_4$," *An. Asoc. Quim. Argentina*, **51**, 43 (1963).

Calderbank, P. H., "Physical Rate Processes in Industrial Fermentation: I. the Interfacial Area in Gas-Liquid Contacting with Mechanical Agitation," *Trans. Inst. Chem. Engrs.*, **36**, 443 (1958).

Camacho, F., E. Molina, F. Valdés, and J. M. Andujar, "Determinación de Areas Interfaciales en Tanques de Burbujeo Agitados: Influencia de las Variables de Operación," *An. Quim.*, **84**, 99 (1988).

Charpentier, J. C., "What's New in Absorption with Chemical Reaction?" *Trans. ICHemE*, **60**, 131 (1982).

Danckwerts, P. V., *Gas-Liquid Reactions*, p. 120, McGraw-Hill, New York (1970).
Hassan, I. T. M., and C. W. Robinson, "Stirred-Tank Mechanical Power Requirement and Gas Holdup in Aerated Aqueous Phases," *AIChEJ.*, **23**, 48 (1977).
Hikita, H., S. Asai, H. Ishikawa, M. Seko, and H. Kitajima, "Diffusivities of Carbon Dioxide in Aqueous Mixed Electrolyte Solutions," *Chem. Eng. J.*, **17**, 77 (1979).
Lee, V. H., and S. Luck, *Annual Reports on Fermentation Processes*, Vol. 6, p. 101, G. Tsao, ed., Academic Press (1983).
Linek, V., and J. Tvrdik, "A Generalization of Kinetic Data on Sulphite Oxidation Systems," *Biotech. Bioeng.*, **13**, 353 (1971).
Linek, V., and V. Vacek, "Chemical Engineering Use of Catalyzed Sulfite Oxidation Kinetics for the Determination of Mass Transfer Characteristics of Gas-Liquid Contactors," *Chem. Eng. Sci.*, **36**, 1747 (1981).
Matheron, E. R., and O. C. Sandall, "Effective Interfacial Area Determination by Gas Absorption Accompanied by Second-Order Irreversible Chemical Reaction," *AIChE J.*, **25**, 332 (1979).
Michel, B. J., and C. A. Miller, "Power Requirements of Gas-Liquid Agitated Systems," *AIChE J.*, **8**, 262 (1962).
Miller, D. N., "Scale-Up of Agitated Vessels Gas-Liquid Mass Transfer," *AIChE J.*, **20**, 445 (1974).
Onda, K., T. Kobayashi, E. Sada, and M. Fujimi, "The Rate of Oxidation of Sodium Sulphite Solution by the Wetted-Wall Column," *Chem. Eng. Japan*, **34**, 187 (1970).
Reith, T., and W. J. Beek, "The Oxidation of Aqueous Sodium Sulphite Solutions," *Chem. Eng. Sci.*, **28**, 1331 (1973).
Robinson, C. W., and C. Wilke, "Oxygen Absorption in Stirred Tanks: a correlation for Ionic Strength Effects," *Biotech. Bioeng.*, **15**, 755 (1973).
Roxburg, J. M., "Studies on Fermentation Aeration: II. Catalyst Effects on Sulphite Oxidation Rates," *Can. J. Chem. Eng.*, **40**, 127 (1962).
Sillen, L. G., *Stability Constants of Metal-Ion Complexes*, Suppl. No. 1, Special Pub. No. 25, Chemical Society of London. p. 23, Oxford (1971).
Sridhar, T., and O. E. Potter, "Gas Holdup and Bubble Diameters in Pressurized Gas-Liquid Stirred Vessels," *Ind. Eng. Chem. Fundam.*, **19**, 21 (1980).
Trushanov, V. N., A. M. Tsirlin, and G. Y. Khodov, "Kinetics of Na_2SO_3 Oxidation in Aqueous Solution in Presence of Cobalt Ions," *J. Appl. Chem. U.S.S.R.*, **48**, 297 (1975).
De Waal, K. J. A., and J. C. Okenson, "The Oxidation of Aqueous Sodium Sulphite Solutions," *Chem. Eng. Sci.*, **21**, 559 (1966).
Westerterp, K. R., L. L. Van Dierendonck, and J. A. De Kraa, "Interfacial Areas in Agitated Gas-Liquid Contactors," *Chem. Eng. Sci.*, **18**, 157 (1963).
Yasunishi, A., "Effect of pH on Oxidation of Aqueous Sodium Sulphite Solutions," *Chem. Eng. Japan*, **3**, 154 (1977).
Yoshida, F., and Y. Miura, "Gas Absorption in Agitated Gas-Liquid Contactors," *Ind. Eng. Chem. Process Des. and Dev.*, **2**, 263 (1963).

Manuscript received May 21, 1990, and revision received June 24, 1991.